ACS Sustainable Chemistry & Engineering

Research Article

pubs.acs.org/journal/ascecg

Synthesis of β-Cyclodextrin-Modified Cellulose Nanocrystals (CNCs)@Fe_3O_4@SiO_2 Superparamagnetic Nanorods

Li Chen,[†] Richard M. Berry,[‡] and Kam C. Tam*[,†]

[†]Department of Chemical Engineering, Waterloo Institute for Nanotechnology, University of Waterloo, 200 University Ave. W, Waterloo, Ontario, Canada N2L 3G1

[‡]CelluForce, Inc., 625 Président-Kennedy Ave., Montreal, Quebec, Canada H3A 1K2

Supporting Information

ABSTRACT: This paper reports on the synthesis of β-cyclodextrin-modified CNC@Fe_3O_4@SiO_2 superparamagnetic nanorods for the removal of two model compounds: procaine hydrochloride and imipramine hydrochloride. During the synthetic process, sustainable natural materials and low-cost chemicals were used, and mild reaction conditions were adopted. TEM and SEM images indicated good dispersion of Fe_3O_4 nanoparticles with uniform silica coating on CNCs. The thickness of the silica coating was controlled by manipulating the amounts of precursor solution used. TGA data confirmed that the silica coating significantly enhanced the thermal stability of CNCs. The onset decomposition temperature of CNC@Fe_3O_4@SiO_2 hybrids increased by 60 °C compared to pure CNCs. XRD, EDS, and FT-IR analyses confirmed the structure of CNC@Fe_3O_4@SiO_2 and the successful grafting of β-cyclodextrin. The CNC@Fe_3O_4@SiO_2@β-CD hybrids displayed good adsorption toward the model pharmaceutical residues: procaine hydrochloride and imipramine hydrochloride.

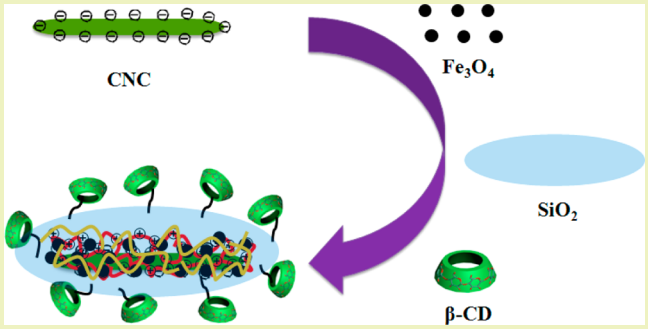

KEYWORDS: *Cellulose nanocrystals, Silica coating, β-Cyclodextrin, Magnetic separation, Drug removal*

INTRODUCTION

Pharmaceutical residues in the aquatic environment have been attracting increasing attention worldwide due to their long-term potential risk to ecosystems and human health.[1,2] Effluent discharge from pharmaceutical manufacturing facilities is considered one of the major sources of contaminants in the environment.[3] In addition, toxic contaminants from manufacturing operations (e.g., chemical plants) and human activities (e.g., using detergents, shampoos, pesticides, and fertilizers) continue to accumulate in our water systems, both at the surface (e.g., rivers and reservoirs) and underground (e.g., aquifers). While many approaches have been developed to eliminate these pollutants, such as electrochemical oxidation, photoelectrocatalysis, and nonthermal plasma,[1] physical adsorption is considered an attractive solution due to its low cost and simple process design.[4] As a rapid and effective technique, magnetic separation can be used to remove various types of organic contaminants.[5] To achieve this, an effective protocol in fabricating magnetic nanoparticles that are suitable for the removal of pharmaceutical contaminants is required.

Superparamagnetic iron oxide nanoparticles have been widely used in numerous applications, such as magnetic resonance image contrast agents,[6] magnetic ferrofluids for hyperthermia,[7] targeted drug delivery,[8] and magnetically assisted separation.[9] However, aggregation and oxidation of iron oxide nanoparticles in a water and oxygen environment significantly reduce their superparamagnetic properties. Although coating the particles with a nonreactive shell as an oxygen barrier is common, it suffers from several shortcomings, most notably the reduction in the magnetic properties of iron nanoparticles. Recently, there are several reported studies on the use of controlled silica coating, where the superparamagnetic property of the nanoparticle is preserved.[10] However, silica-coated magnetic nanoparticles tend to aggregate into irregular or nonuniform shapes making the synthesis a significant challenge.[11]

Hybrid inorganic−organic nanocomposite materials are of practical interest due to their multifunctionality, processability, and potential large-scale production.[12] Cellulose nanocrystals (CNCs) are attracting increasing interest due to their uniform nanorod shape, good mechanical strength, liquid crystalline character, high specific surface area, biocompatibility, biodegradability, and sustainability.[13,14] In addition, it can be produced at an industrial scale by acid hydrolysis of pulp fibers. CNCs consist of hydrogen-bonded linear chains of β-D-glucopyranose bundled together to form nanorods with diameters of 10−20 nm and lengths of 200−400 nm.[15] The negative charge and hydroxyl groups on the surface of CNCs make them good template materials for noble metal nanoparticles (e.g., Au,[16] Ag,[17] Pd[18]). However, there is currently

Received: December 18, 2013
Revised: February 21, 2014
Published: February 25, 2014

Scheme 1. Schematic Representation for the Synthesis of CNC@Fe_3O_4@SiO_2@ β-CD[a]

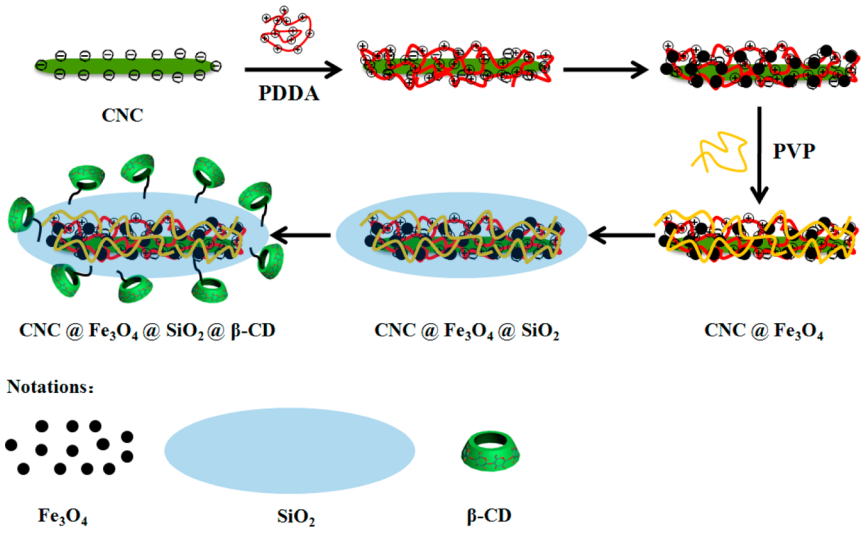

[a]CNC: cellulose nanocrystal. PDDA: poly(diallydimethylammonium chloride). PVP: polyvinylpyrrolidone. β-CD: β-cyclodextrin.

limited study on the preparation of iron oxide nanoparticles on the surface of CNCs.

Recently, silica-CNCs composites have aroused great interest and were applied to obtain chiral nematic mesoporous carbons[19,20] and carbon needles,[21] where silica served as frameworks and robust nanoreactors, respectively. Here, we have chosen CNCs and silica as supporting template and coating materials, respectively, for iron oxide nanoparticles, and we propose strategies to address the issues relating to aggregation and oxidation of the magnetic nanorods. The proposed system would exhibit the following attractive features: (1) CNCs and silica are abundant, and they are environmentally friendly and biocompatible. (2) Silica coating is controllable and can enhance the thermal stability of CNCs. (3) Silica can further be modified due to the abundance of hydroxyl groups.

β-Cyclodextrin (β-CD) has been extensively investigated in the pharmaceutical industry[22] as food additives[23] and for water treatment[24] due to its special structure, biocompatibility, and low cost. Here, we grafted β-CD onto the surface of CNC@Fe_3O_4@SiO_2 hybrids and explored their application in the adsorption of two model organic compounds: procaine hydrochloride and imipramine hydrochloride.

EXPERIMENTAL SECTION

Materials. CNCs were supplied by CelluForce, Inc. Ammonia and ethanol were purchased from Fisher Scientific. Aqueous solutions of poly(diallydimethylammonium chloride) (20% PDDA, MW: 100,000−200,000), polyvinylpyrrolidone (PVP, MW: 10,000), β-cyclodextrin, NaOH, $NaHCO_3$, toluene, and cyanuric chloride were purchased from Sigma Aldrich. Tetraethyl orthosilicate (98%) and 3-aminopropyl-triethoxysilane (99%) were purchased from Acros Organics. All the chemicals were used without further purification. Purified water from a Milli-Q Millipore system (>18 MΩ cm) was used in preparing the sample solutions.

Methods. The preparation of CNC@Fe_3O_4@SiO_2@β-CD comprises six steps as shown in Scheme 1. Details on the synthesis of CNC@Fe_3O_4@SiO_2 hybrids with different thicknesses of silica shell are summarized in Table 1.

Synthesis of Fe_3O_4 Nanoparticles. Fe_3O_4 nanoparticles were synthesized by co-precipitation of Fe^{2+} and Fe^{3+} cations as previously reported.[25] The co-precipitation overall reaction is described by the chemical reaction scheme[26]

$$Fe^{2+} + 2Fe^{3+} + 8OH^- \rightarrow Fe_3O_4 + 4H_2O$$

In a typical procedure, 0.24 g of $Fe_3(NO_3)_3{\cdot}9H_2O$ and 0.08 g of $FeSO_4{\cdot}7H_2O$ were dissolved in 15 mL of water, and then 10 mL of 1 N HCl was added. The homogeneous solution obtained was added dropwise into 100 mL of a 1.5 M NaOH solution under vigorous stirring in the presence of a nitrogen blanket. Then, 1.0 g of PVP 10 was added; the adsorbed PVP enhanced the stability of the Fe_3O_4 nanoparticles through steric repulsive forces. The precipitate was washed four times using a high gradient magnetic separator (HGMS), and the particles were redispersed in deoxygenated ethanol.

Synthesis of CNC@Fe_3O_4. As PDDA and PVP have been widely used in the fabrication of various types of nanoparticles,[27,28] they were used here in the synthesis CNC@Fe_3O_4. CNCs with diameters of 10−20 nm and lengths of 200−400 nm were used without further treatment (Figure S1, Supporting Information). To immobilize Fe_3O_4 onto CNCs, 0.15 g of CNCs were first dispersed in 100 mL of a water solution containing 0.5 mL of PDDA. The solution suspension was stirred on a magnetic stirrer and incubated for 16 h to obtain PDDA-modified CNCs. Then, 0.02 g of Fe_3O_4 nanoparticles were added, and the suspension was stirred for another 4 h after which 0.15 g of PVP 10 was added. After 16 h, PVP-capped CNC@Fe_3O_4 was recovered via centrifugation at 4000 rpm for 15 min. The TEM of CNC@Fe_3O_4 confirmed the successful synthesis of a well-dispersed iron oxide nanoparticle/CNC system (Figure S2, Supporting Information).

Synthesis of CNC@Fe_3O_4@SiO_2. The precipitates obtained previously were redispersed in ethanol/H_2O (80 mL/20 mL) solution,

Table 1. Summary of Notation and Composition for the Synthesis of CNC@Fe_3O_4@SiO_2 Hybrids with Controllable Thicknesses of Silica Coating

nanocomposites	CNC (g)	PDDA (mL)	Fe_3O_4 (g)	PVP (g)	TEOS (μL)
CNC@Fe_3O_4	0.15	0.5	0.02	0.15	0
CNC@Fe_3O_4@SiO_2−50	0.15	0.5	0.02	0.15	50
CNC@Fe_3O_4@SiO_2−100	0.15	0.5	0.02	0.15	100
CNC@Fe_3O_4@SiO_2−150	0.15	0.5	0.02	0.15	150
CNC@Fe_3O_4@SiO_2−200	0.15	0.5	0.02	0.15	200

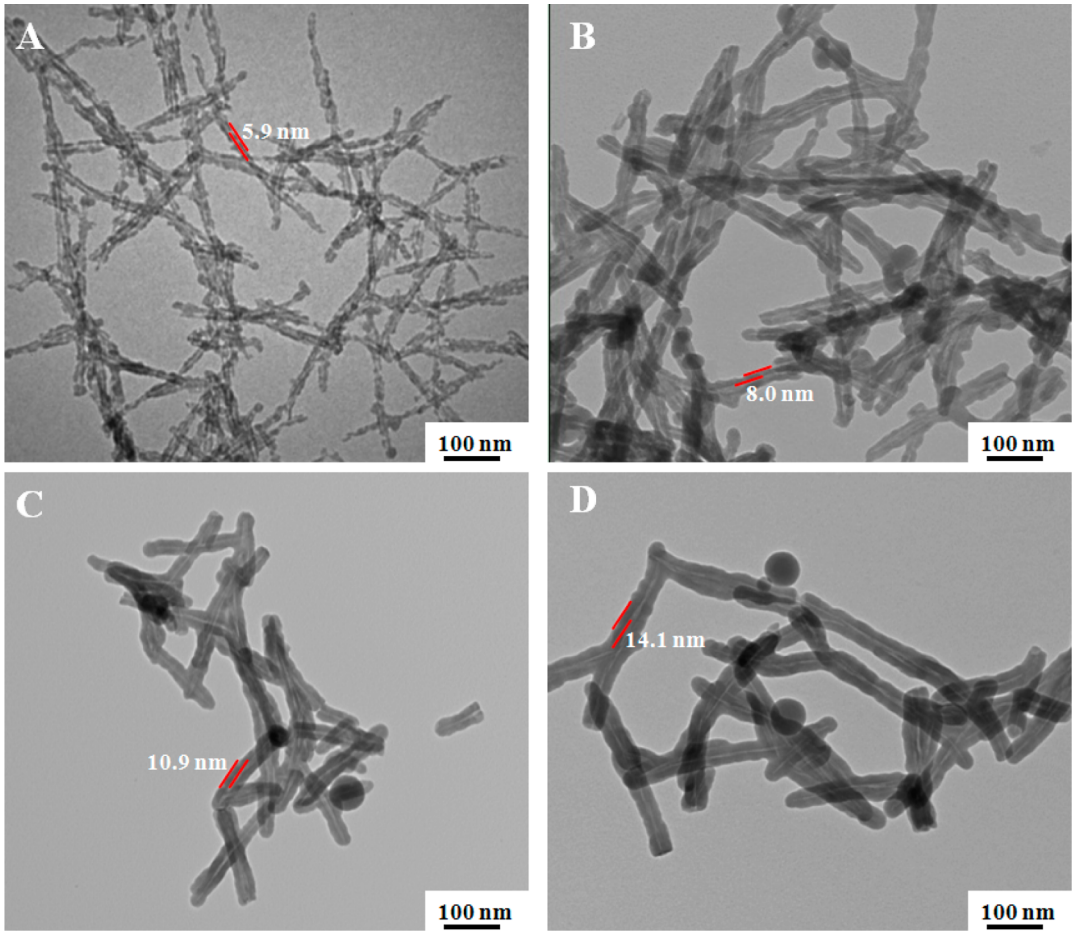

Figure 1. TEM images of CNC@Fe_3O_4@SiO_2-50 (A), CNC@Fe_3O_4@SiO_2-100 (B), CNC@Fe_3O_4@SiO_2-150 (C), and CNC@Fe_3O_4@SiO_2-200 (D).

and then 10 mL of dilute ammonia solution (4.2% in ethanol) and various amounts of TEOS were added (Table 1). The reaction mixture was allowed to react at room temperature under continuous stirring for 20 h. The product was separated and purified by decantation and freeze-dried.

Synthesis of CNC@Fe_3O_4@SiO_2@β-CD. Monochlorotriazine-β-CD (MCT-β-CD) was synthesized according to previously published work,[29,30] and it was then used to graft onto the CNC@Fe_3O_4@SiO_2 hybrid nanostructures. The structure of MCT-β-CD is shown in Figure S3 of the Supporting Information, which was confirmed by FTIR and ESI-MS analyses (Figures S4 and S5, Supporting Information). First, the silica shell was functionalized with primary amines and then reacted with MCT-β-CD. Typically, 150 mg of CNC@Fe_3O_4@SiO_2-100 was dispersed in a solution of 50 mL of toluene and 150 μL of 3-aminopropyltrimethoxysilane (APTEOS). The solution was kept at 80 °C and stirred under nitrogen for 2 h. The aminated CNC@Fe_3O_4@SiO_2-100 was thoroughly washed, purified by decantation, and then freeze-dried. Then, 150 mg of aminated CNC@Fe_3O_4@SiO_2-100 was dissolved in 50 mL of water containing 300 mg of MCT-β-CD, and a saturated solution of $NaHCO_3$ was introduced into the solution to maintain a pH of 8. After 24 h, the product was washed, separated by decantation, and freeze-dried.

Depollution Procedure. Adsorption tests were carried out in 20 mL beakers. In each beaker, 10 mL of an aqueous solution containing 23.6 ppm procaine hydrochloride and 10 mg of CNC@Fe_3O_4@SiO_2-100@β-CD or CNC@Fe_3O_4@SiO_2-100 as adsorbents were thoroughly mixed. The mixture was stirred for 5 min before passing through the HGMS at a flow rate of 0.25 mL/s. The magnetic field of 1.0 T was applied for the separation process. The magnetic nanoparticles were retained in the high gradient magnetic separator (HGMS), while unbound organic compounds in the form of a clear solution were collected and measured by UV−vis spectroscopy. After the measurement, the magnetic nanoparticles and the clear solution were carefully recovered and mixed again. This process was repeated five times until no further reduction in the absorbance was observed.

Characterization. The morphology of CNC@Fe_3O_4@SiO_2 hybrids were evaluated using transmission electron microscopy (TEM). The features of CNC@Fe_3O_4@SiO_2 were observed using a scanning electron microscope (SEM ZEISS) with energy dispersive spectroscopy (SEM-EDS) under an accelerating voltage of 20 kV. X-ray diffraction (XRD) patterns were recorded by a Rigaku XRD-6000 diffractometer, using Cu Kα radiation (λ = 0.154 nm) at 40 kV, 30 mA. Fourier-transform infrared (FT-IR) spectroscopy was used to study the chemical composition of CNC@Fe_3O_4@SiO_2 nanocomposites. The magnetic properties of the samples were characterized with a Lake Shore 7410 vibrating sample magnetometer. Mass spectrometry (Q-TOF Ultima Global, Waters, the University of Waterloo Mass Spectrometry Facility) was applied to confirm the synthesis of MCT-β-CD. A high gradient magnetic separator (HGMS) (Frantz Isodynamic Magnetic Separator-Model-1, Frantz, Inc.) was used to recover the magnetic nanoparticles in the study on the removal of model organic compounds. The UV−vis spectra were obtained using a Shimadzu U-3000 spectrophotometer.

RESULTS AND DISCUSSION

The CNC@Fe_3O_4@SiO_2 containing various silica coatings of varying thicknesses were obtained by controlling the amounts of TEOS added during the coating process (Table 1). The morphology and architecture of CNC@Fe_3O_4@SiO_2 were investigated using TEM and SEM. The TEM images confirmed the homogeneous dispersion of Fe_3O_4 nanoparticles on the

dx.doi.org/10.1021/sc400540f | ACS Sustainable Chem. Eng. 2014, 2, 951−958

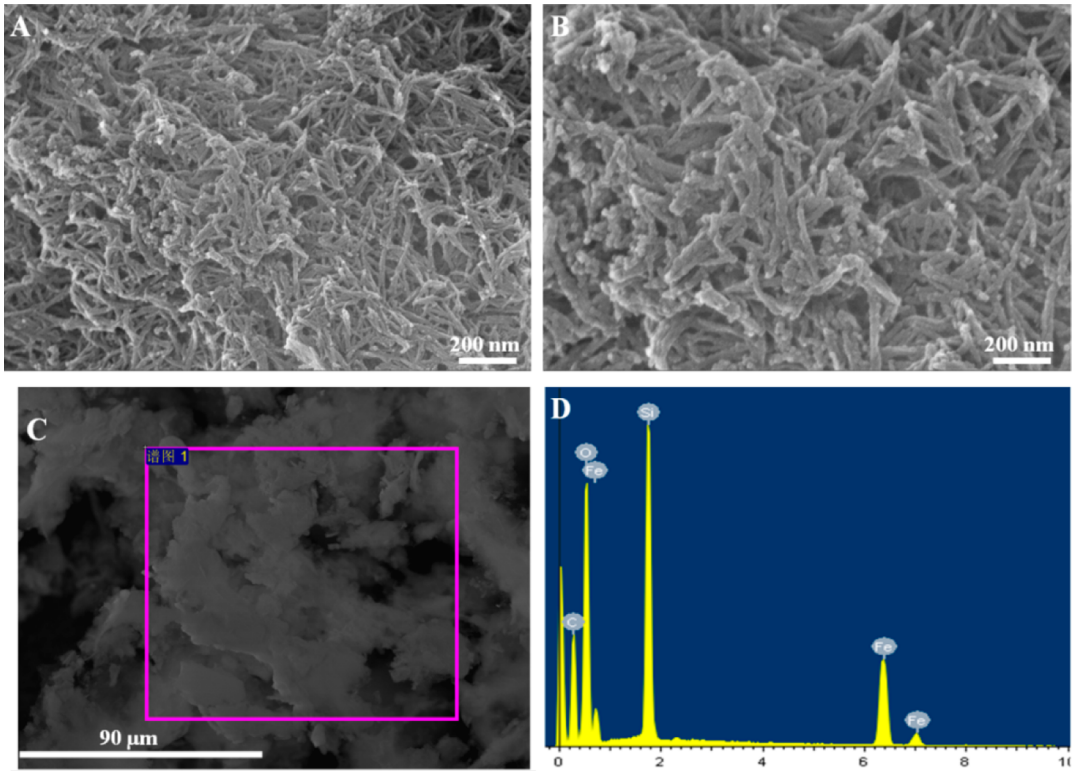

Figure 2. SEM images for the CNC@Fe_3O_4@SiO_2-100: low magnification (A) and high magnification (B). SEM image (C) and corresponding EDX data (D) for the CNC@Fe_3O_4@SiO_2-100.

surface of CNC and the uniform silica coating on the CNC@Fe_3O_4 hybrid nanostructure. Because of the contrast between the various components, a distinct core−shell structure was observed for the CNC@Fe_3O_4@SiO_2 hybrid systems. When the amounts of TEOS added was increased from 50 μL (Figure 1A) to 200 μL (Figure 1D), the thickness of the silica coating increased correspondingly. The shell thickness for samples A−D was determined to be 5.9, 8.0, 10.9, and 14.1 nm, respectively. In addition, no obvious aggregation of CNCs and Fe_3O_4 nanoparticles was observed. However, due to excess of TEOS, small amounts of spherical silica spheres were evident as indicated in Figure 1C and D. It was previously reported that thin silica coatings obtained via the Stöber method were not homogeneous and could be unstable, where the coating could be redissolved when the nanoparticles were stored in an aqueous solution for a prolonged period of time.[31] From this study, the optimum sample CNC@Fe_3O_4@SiO_2-100 was selected for further characterization and for subsequent grafting of β-CD.

The top view SEM images of CNC@Fe_3O_4@SiO_2 exhibited uniform rod-like structures (Figure 2A and B). Meanwhile, CNC@Fe_3O_4@SiO_2 nanocomposites did not contain any large aggregates (Figure 2C) in contrast to Fe_3O_4 nanoparticles where larger aggregates were evident (Figures S6 and S7, Supporting Information). To further confirm the structure of CNC@Fe_3O_4@SiO_2 nanocomposites, SEM and EDX were used to measure the atomic species present in CNC@Fe_3O_4@SiO_2-100, and the elements C, O, Si, and Fe were detected. On the basis of EDX analysis, the SiO_2/Fe_3O_4 molar ratio for CNC@Fe_3O_4@ SiO_2-100 was calculated to be 8.22.

The influence of varying the amounts of TEOS on the CNC@Fe_3O_4@SiO_2 hybrids was analyzed by FT-IR (Figure 3). Compared to CNCs, new absorbance bands at 789 and 450

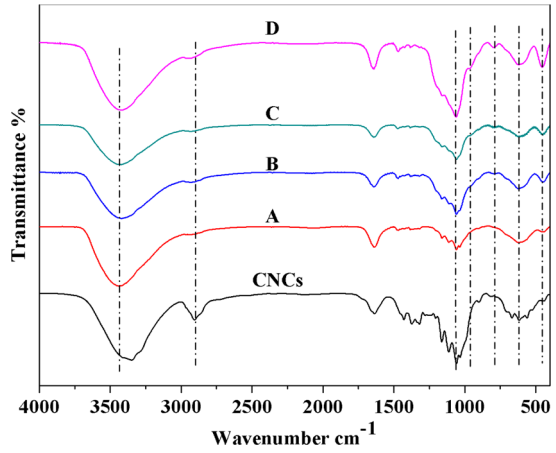

Figure 3. FT-IR spectra of CNCs: CNC@Fe_3O_4@SiO_2-50 (A), CNC@Fe_3O_4@SiO_2-100 (B), CNC@Fe_3O_4@SiO_2-150 (C), and CNC@Fe_3O_4@SiO_2-200 (D).

cm^{-1} corresponding to the symmetric stretching vibrations and the bending mode of Si−O−Si were detected. The band centered at 960 cm^{-1} is due to the Si−O in-plane stretching vibrations of the silanol groups. The bands in the range of 1200−1000 cm^{-1} assigned to the Si−O covalent bond vibrations further confirmed the formation of a dense silica network.[32] In addition, the characteristic band at 620 cm^{-1} is attributed to the asymmetric stretching vibration of Fe−O appearing in the FTIR spectra of CNC@Fe_3O_4@SiO_2 hybrids.[33] Further, CNCs displayed distinct peaks at 2907 and 2855 cm^{-1} that are assigned to C−H asymmetric and symmetric stretching vibrations, while CNC@Fe_3O_4@SiO_2 hybrids showed small peaks in these wavenumbers due to

dx.doi.org/10.1021/sc400540f | ACS Sustainable Chem. Eng. 2014, 2, 951−958

nonhydrolyzed alkoxy groups on the silica surface.[34] In general, the absorbance bands of silica became sharper and more obvious with increasing amounts of TEOS added to the reaction mixtures, while the bands of CNCs decreased or disappeared. These trends confirmed the existence of Fe_3O_4 and the increasing thicknesses of the silica shells from A to D.

To further confirm the formation of the silica-coated CNC@Fe_3O_4 core−shell structure, XRD was employed to examine the crystal structure of the samples (Figure 4). The Fe_3O_4

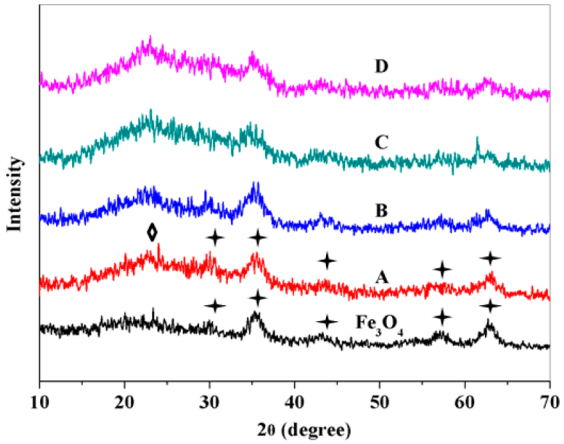

Figure 4. XRD patterns of Fe_3O_4 nanoparticles: CNC@Fe_3O_4@SiO_2-50 (A), CNC@ Fe_3O_4@SiO_2-100 (B), CNC@Fe_3O_4@SiO_2-150 (C), and CNC@Fe_3O_4@SiO_2-200 (D).

nanoparticles exhibited well-resolved peaks at 30.0°, 35.4°, 43.2°, 57.0°, and 62.7°, which are attributed to (220), (311), (400), (422), (511), and (440) reflections of Fe_3O_4, respectively.[35] For CNC@Fe_3O_4@SiO_2 hybrids, new broad reflection profiles centered at 22.5° should be ascribed to the amorphous silica.[36] The data showed that CNC@Fe_3O_4@SiO_2 hybrids possessed diffraction peaks of Fe_3O_4 nanoparticles and amorphous SiO_2. Cellulose nanocrystals are crystalline, and the XRD pattern of CNCs exhibits diffractions at 15.2°, 23.0°, and 34.8° (Figure S8, Supporting Information). However, there are no obvious diffraction peaks from CNCs in the hybrids, which is probably due to the considerable difference in the atomic scattering factors.[37] In addition, liquid ammonia used as the catalyst for the silica coating at 25 °C may have altered the crystalline structure of CNCs,[38] which further reduced the diffraction pattern of the CNCs. Together with the results from TEM and SEM, we could conclude that Fe_3O_4 nanoparticles were encapsulated within the silica shells.

The magnetic properties of CNC@Fe_3O_4@SiO_2 hybrids with different silica shell thicknesses were studied with a vibrating sample magnetometer at 300 K. The hysteresis loops revealed that both the Fe_3O_4 and CNC@Fe_3O_4@SiO_2 hybrids displayed low coercivity with no obvious hysteresis confirming the superparamagnetism of the hybrid systems. Due to the superparamagnetic property, the CNC@Fe_3O_4@SiO_2 hybrids exhibited a fast response to an external magnetic field and quickly redispersed under slight shaking once the magnetic field was removed (Figure 5.). The reversible process is an advantage in many applications. In addition, the magnetization value at 20 kOe for Fe_3O_4 was 67 emu/g (Figure S9, Supporting Information). With increasing amounts of TEOS, the magnetization value of the CNC@Fe_3O_4@SiO_2 hybrids decreased

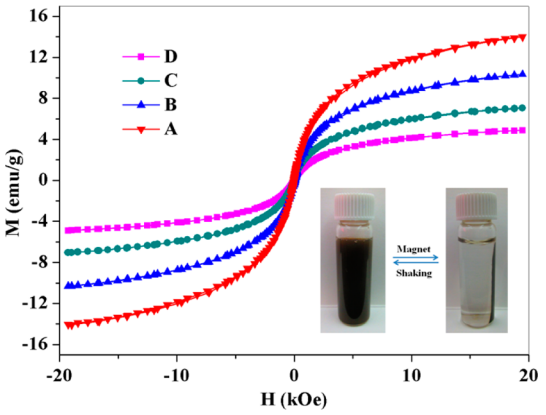

Figure 5. Room-temperature (300 K) magnetic hysteresis loops of CNC@Fe_3O_4@SiO_2-50 (A), CNC@Fe_3O_4@SiO_2-100 (B), CNC@Fe_3O_4@SiO_2-150 (C), and CNC@Fe_3O_4@SiO_2-200 (D).

from 14.0 to 10.3 to 7.0 to 5.0 emu/g, which further confirmed the increasing thicknesses of the silica coating on CNC@Fe_3O_4.

The thermal stability of CNCs and CNC@Fe_3O_4@SiO_2 hybrids was measured by thermogravimetric analysis (TGA) under N_2 at a heating rate of 10 °C/min. The TGA plot in Figure S10 of the Supporting Information demonstrates that CNC started to decompose at 260 °C resulting in a weight loss of 56%. As for the CNC@Fe_3O_4@SiO_2 systems, the weight loss between room temperature to 320 °C was due to the absorbed water and dehydroxylation on the surface and interior of the silica.[39] The thermal onset for the decomposition of CNC@Fe_3O_4@SiO_2 hybrids was shifted from 260 to 320 °C, indicating that silica coating served as a thermal barrier[40] and thus greatly enhanced the thermal stability of CNCs.

In this section, CNC@Fe_3O_4@SiO_2-100 was chosen as the optimum hybrid for further modification with MCT-β-CD to produce the CNC@Fe_3O_4@SiO_2-100@β-CD system. The FTIR spectrum of β-CD revealed three typical peaks at 1157, 1080, and 1031 cm^{-1}.[41] Compared with the spectrum of β-CD, the FTIR spectrum of MCT-β-CD displayed a new peak at 1112 cm^{-1}, which corresponded to the C−O−C stretching vibration. Other new bands at 1579, 1464, 1293, 1255, and 820 cm^{-1} can be assigned to the triazinyl ring[42,43] (Figure S4, Supporting Information). As for the FT-IR of the synthesized CNC@Fe_3O_4@SiO_2-100@β-CD nanocomposites (Figure 6),

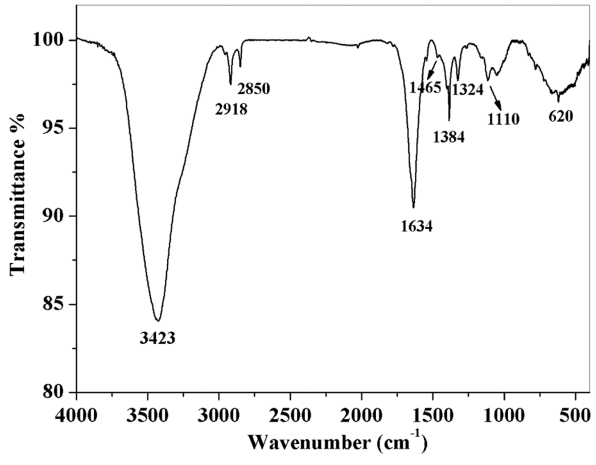

Figure 6. FT-IR of β-CD-modified CNC@Fe_3O_4@SiO_2-100.

dx.doi.org/10.1021/sc400540f | ACS Sustainable Chem. Eng. 2014, 2, 951−958

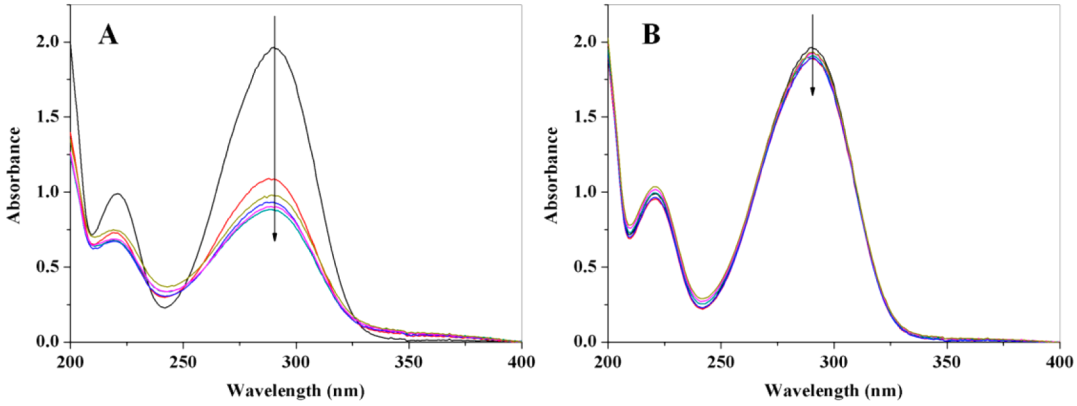

Figure 7. UV−vis of the upper clear procaine solution in 10 mg of CNC@Fe_3O_4@SiO_2-100@β-CD (A) and in 10 mg of CNC@Fe_3O_4@SiO_2-100 (B) with different adsorption times.

the sharp peaks at 706 and 757 cm^{-1}, assigned to the stretching vibration υ(C−Cl),[44] disappeared in the grafted products, confirming the reaction between MCT-β-CD and modified CNC@Fe_3O_4@SiO_2. C−H asymmetric and symmetric stretching vibrations appeared at 2918 and 2850 cm^{-1}, which can be attributed to the carbon chain between the silica surface and β-CD. In addition, the vibrations of the triazinyl ring (1465 cm^{-1}), Fe−O (620 cm^{-1}), Si−O (1110 cm^{-1}) were observed. These results confirmed that β-CD was successfully grafted on the surface of CNC@Fe_3O_4@SiO_2-100.

The behavior of CNC@Fe_3O_4@SiO_2-100@β-CD in removing model organic compounds (Figure S11, Supporting Information) was investigated by UV−vis spectroscopy. In order to study the adsorption process, a control CNC@Fe_3O_4@SiO_2-100 was also tested under similar conditions. Typically, the adsorption tests were carried out in 20 mL beakers. In each beaker, 10 mL of an aqueous solution containing 23.6 ppm procaine hydrochloride and 10 mg of CNC@Fe_3O_4@SiO_2-100@β-CD or CNC@Fe_3O_4@SiO_2-100 as adsorbents were added. The mixed solution was stirred for 5 min, and then the samples were passed through the HGMS, where the magnetic nanoparticles were retained in the HGMS and unbound organic compounds in the form of a clear solution were recovered. The concentration of the supernatant in the filtered solution was monitored by UV−vis spectroscopy. This adsorption/separation process was repeated several times until the value of the absorbance approached a stable value. The UV−vis data indicate there is no obvious change of absorbance of the supernatant for the procaine hydrochloride solution in the 10 mg CNC@Fe_3O_4@SiO_2-100 sample, while fast adsorption of procaine hydrochloride by CNC@Fe_3O_4@SiO_2-100@β-CD was observed (Figure 7). These results further confirmed the successful synthesis of CNC@Fe_3O_4@SiO_2-100@β-CD. The adsorption capacity was determined to be 13.0 ± 0.09 mg/g. A similar phenomenon was also observed for removal of imipramine hydrochloride with an adsorption capacity of 14.8 ± 0.16 mg/g (Figure S12, Supporting Information). The final concentrations for procaine hydrochloride and imipramine hydrochloride were 10.6 and 11.1 ppm, respectively. Compared with conventional membrane separations that generally suffer from fouling, poor permeate quality, and low flux enhancement,[45] the magnetic separation shows several advantages including rapid process (short residence time and fast kinetics), simple cleanup, and easy recovery of adsorbents. In addition, the flow rate of the mixture of polluted water and magnetic particles can be easily adjusted and increased using various diameter tubes.

CONCLUSIONS

A β-CD-modified CNC@Fe_3O_4@SiO_2-100 inorganic−organic hybrid was successfully prepared. TEM, SEM-EDX, XRD, and FT-IR analyses confirmed its core−shell structure. The structural morphology studies indicated that there is no obvious aggregation of Fe_3O_4 on the CNCs, and the thicknesses of silica could be controlled by varying the amounts of TEOS. The TGA spectra revealed that the silica coating could significantly enhance the thermal stability of CNCs, where the onset decomposition temperature was increased by 60 °C. Furthermore, the as-prepared CNC@Fe_3O_4@SiO_2-100@β-CD hybrid displayed a good magnetic property and effective adsorption characteristic toward two model organic compounds. Therefore, the CNC@Fe_3O_4@SiO_2-100@β-CD inorganic−organic hybrid can be potentially applied for the removal of pharmaceutical residues. Finally, the procedure reported here can be extended to prepare other inorganic−organic nanocomposites using CNCs as the template material.

ASSOCIATED CONTENT

Supporting Information

Structure, synthesis, and characterization of MCT-β-CD; TEM images of CNC, Fe_3O_4, and CNC@ Fe_3O_4; SEM-EDX of Fe_3O_4; XRD of CNC; room-temperature magnetic hysteresis loop for Fe_3O_4; structure of procaine hydrochloride and imipramine hydrochloride; and adsorption behavior for imipramine hydrochloride. This material is available free of charge via the Internet at http://pubs.acs.org.

AUTHOR INFORMATION

Corresponding Author

*Tel.: 519-888-4567, ext. 38339. Fax: 519-888-4347. E-mail: mkctam@uwaterloo.ca.

Notes

The authors declare no competing financial interest.

ACKNOWLEDGMENTS

We wish to acknowledge FP Innovations for providing the first batch of freezed dried CNC sample. The research funding from CelluForce and AboraNano facilitated the research on CNC. K.C.T. wishes to acknowledge funding from CFI and NSERC.

REFERENCES

(1) Sirés, I.; Brillas, E. Remediation of water pollution caused by pharmaceutical residues based on electrochemical separation and degradation technologies: A review. *Environ. Int.* **2012**, *40*, 212−229.

(2) Fatta-Kassinos, D.; Meric, S.; Nikolaou, A. Pharmaceutical residues in environmental waters and wastewater: current state of knowledge and future research. *Anal. Bioanal. Chem.* **2011**, *399*, 251−275.

(3) Larsson, D. G. J.; Fick, J. Transparency throughout the production chain—A way to reduce pollution from the manufacturing of pharmaceuticals? *Regul. Toxicol. Pharmacol.* **2009**, *53*, 161−163.

(4) Blöcher, C. Elimination of micropollutants and hazardous substances at the source in the chemical and pharmaceutical industry. *Water Sci. Technol.* **2007**, *56*, 119−123.

(5) Ai, L.; Huang, H.; Chen, Z.; Wei, X.; Jiang, J. Activated carbon/$CoFe_2O_4$ composites: Facile synthesis, magnetic performance and their potential application for the removal of malachite green from water. *Chem. Eng. J.* **2010**, *156*, 243−249.

(6) Lee, H.; Lee, E.; Kim, D. K.; Jang, N. K.; Jeong, Y. Y.; Jon, S. Antibiofouling polymer-coated superparamagnetic iron oxide nanoparticles as potential magnetic resonance contrast agents for in vivo cancer imaging. *J. Am. Chem. Soc.* **2006**, *128*, 7383−7389.

(7) Hayashi, K.; Moriya, M.; Sakamoto, W.; Yogo, T. Chemoselective synthesis of folic acid-functionalized magnetite nanoparticles via click chemistry for magnetic hyperthermia. *Chem. Mater.* **2009**, *21*, 1318−1325.

(8) Cheng, K.; Peng, S.; Xu, C.; Sun, S. Porous hollow Fe_3O_4 nanoparticles for targeted delivery and controlled release of cisplatin. *J. Am. Chem. Soc.* **2009**, *131*, 10637−10644.

(9) Bao, J.; Chen, W.; Liu, T.; Zhu, Y.; Jin, P.; Wang, L.; Liu, J.; Wei, Y.; Li, Y. Bifunctional Au-Fe_3O_4 nanoparticles for protein separation. *ACS Nano.* **2007**, *1*, 293−298.

(10) He, Y. P.; Wang, S. Q.; Li, C. R.; Miao, Y. M.; Wu, Z. Y.; Zou, B. S. Synthesis and characterization of functionalized silica-coated Fe_3O_4 superparamagnetic nanocrystals for biological applications. *J. Phys. D: Appl. Phys.* **2005**, *38*, 1342−1350.

(11) Santra, S.; Tapec, R.; Theodoropoulou, N.; Dobson, J.; Hebard, A.; Tan, W. Synthesis and characterization of silica-coated iron oxide nanoparticles in microemulsion: The effect of nonionic surfactants. *Langmuir* **2001**, *17*, 2900−2906.

(12) Gass, J.; Poddar, P.; Almand, J.; Srinath, S.; Srikanth, H. Superparamagnetic polymer nanocomposites with uniform Fe_3O_4 nanoparticle dispersions. *Adv. Funct. Mater.* **2006**, *16*, 71−75.

(13) Habibi, Y. Key advances in the chemical modification of nanocelluloses. *Chem. Soc. Rev.* **2014**, *43*, 1519−1542.

(14) Peng, B. L.; Dhar, N.; Liu, H. L.; Tam, K. C. Chemistry and applications of nanocrystalline cellulose and its derivatives: A nanotechnology perspective. *Can. J. Chem. Eng.* **2011**, *89*, 1191−1206.

(15) Siqueira, G.; Bras, J.; Dufresne, A. Cellulosic bionanocomposites: A review of preparation, properties and applications. *Polymers* **2010**, *2*, 728−765.

(16) Koga, H.; Tokunaga, E.; Hidaka, M.; Umemura, Y.; Saito, T.; Isogai, A.; Kitaoka, T. Topochemical synthesis and catalysis of metal nanoparticles exposed on crystalline cellulose nanofibers. *Chem. Commun.* **2010**, *46*, 8567−8569.

(17) Ifuku, S.; Tsuji, M.; Morimoto, M.; Saimoto, H.; Yano, H. Synthesis of silver nanoparticles templated by TEMPO-mediated oxidized bacterial cellulose nanofibers. *Biomacromolecules* **2009**, *10*, 2714−2717.

(18) Cirtiu, C. M.; Dunlop-Brière, A. F.; Moores, A. Cellulose nanocrystallites as an efficient support for nanoparticles of palladium: application for catalytic hydrogenation and Heck coupling under mild conditions. *Green Chem.* **2011**, *13*, 288−291.

(19) Asefa, T. Chiral nematic mesoporous carbons from self-assembled nanocrystalline cellulose. *Angew. Chem., Int. Ed.* **2012**, *51*, 2008−2010.

(20) Shopsowitz, K. E.; Hamad, W. Y.; MacLachlan, M. J. Chiral nematic mesoporous carbon derived from nanocrystalline cellulose. *Angew. Chem., Int. Ed.* **2011**, *50*, 10991−10995.

(21) Silva, R.; Al-Sharab, J.; Asefa, T. Edge-plane-rich nitrogen-doped carbon nanoneedles and efficient metal-free electrocatalysts. *Angew. Chem., Int. Ed.* **2012**, *51*, 7171−7175.

(22) Okamatsu, A.; Motoyama, K.; Onodera, R.; Higashi, T.; Koshigoe, T.; Shimada, Y.; Hattori, K.; Takeuchi, T.; Arima, H. Folate-appended β-cyclodextrin as a promising tumor targeting carrier for antitumor drugs in vitro and in vivo. *Bioconjugate Chem.* **2013**, *24*, 724−733.

(23) Astray, G.; Gonzalez-Barreiro, C.; Mejuto, J. C.; Rial-Otero, R.; Simal-Gándara, J. A review on the use of cyclodextrins in foods. *Food Hydrocolloids* **2009**, *23*, 1631−1640.

(24) Hu, J.; Shao, D.; Chen, C.; Sheng, G.; Li, J.; Wang, X.; Nagatsu, M. Plasma-induced grafting of cyclodextrin onto multiwall carbon nanotube/iron oxides for adsorbent application. *J. Phys. Chem. B* **2010**, *114*, 6779−6785.

(25) Kang, Y. S.; Risbud, S.; Rabolt, J. F.; Stroeve, P. Synthesis and characterization of nanometer-size Fe_3O_4 and γ-Fe_2O_3 particles. *Chem. Mater.* **1996**, *8*, 2209−2211.

(26) Gupta, A. K.; Gupta, M. Synthesis and surface engineering of iron oxide nanoparticles for biomedical applications. *Biomaterials* **2005**, *26*, 3995−4021.

(27) Song, W.; Li, H.; Liu, H.; Wu, Z.; Qiang, W.; Xu, D. Fabrication of streptavidin functionalized silver nanoparticle decorated graphene and its application in disposable electrochemical sensor for immunoglobulin E. *Electrochem. Commun.* **2013**, *31*, 16−19.

(28) Hou, Y.; Li, T.; Huang, H.; Quan, H.; Miao, X.; Yang, M. Electrochemical immunosensor for the detection of tumor necrosis factor α based on hydrogel prepared from ferrocene modified amino acid. *Sens. Actuators, B* **2013**, *182*, 605−609.

(29) Liu, J.; Xu, H.; Shen, L.; Chen, R.; Yu, Z. Synthesis of monochlorotriazinyl-β-cyclodextrin as a novel textile auxiliary. *Adv. Mater. Res.* **2012**, *441*, 431−435.

(30) Reuscher, H.; Hirsenkorn, R. Beta W7MCT-new ways in surface modification. *J. Inclusion Phenom. Mol. Recognit. Chem.* **1996**, *25*, 191−196.

(31) Wong, Y. J.; Zhu, L.; Teo, W. S.; Tan, Y. W.; Yang, Y.; Wang, C.; Chen, H. Revisiting the stober method: inhomogeneity in silica shells. *J. Am. Chem. Soc.* **2011**, *133*, 11422−11425.

(32) Al-Oweini, R.; El-Rassy, H. Synthesis and characterization by FTIR spectroscopy of silica aerogels prepared using several $Si(OR)_4$ and $R''Si(OR')_3$ precursors. *J. Mol. Struct.* **2009**, *919*, 140−145.

(33) Andhariya, N.; Chudasama, B.; Mehta, R. V.; Upadhyay, R. V. Nanoengineering of methylene blue loaded silica encapsulated magnetite nanospheres and nanocapsules for photodynamic therapy. *J. Nanopart. Res.* **2011**, *13*, 3619−3631.

(34) Cao, X.; Habibi, Y.; Lucia, L. A. One-pot polymerization, surface grafting, and processing of waterborne polyurethane-cellulose nanocrystal nanocomposites. *J. Mater. Chem.* **2009**, *19*, 7137−7145.

(35) Seoyoun, S.; Jang, J. Thiol containing polymer encapsulated magnetic nanoparticles as reusable and efficiently separable adsorbent for heavy metal ions. *Chem. Commun.* **2007**, *41*, 4230−4232.

(36) Yang, H.; Zhuang, Y.; Hu, H.; Du, X.; Zhang, C.; Shi, X.; Wu, H.; Yang, S. Silica-coated manganese oxide nanoparticles as a platform for targeted magnetic resonance and fluorescence imaging of cancer cells. *Adv. Funct. Mater.* **2010**, *20*, 1733−1741.

(37) Valant, M.; Axelsson, A. K.; Alford, N. Peculiarities of a solid-state synthesis of multiferroic polycrystalline $BiFeO_3$. *Chem. Mater.* **2007**, *19*, 5431−5436.

(38) Mittal, A.; Katahira, R.; Himmel, M. E.; Johnson, D. K. Effects of alkaline or liquid-ammonia treatment on crystalline cellulose: Changes in crystalline structure and effects on enzymatic digestibility. *Biotechnol. Biofuels* **2011**, *4*, 1−16.

(39) Wang, R.; Baran, G.; Wunder, S. L. Packing and thermal stability of polyoctadecylsiloxane compared with octadecylsilane monolayers. *Langmuir* **2000**, *16*, 6298−6305.

(40) Hribernik, S.; Smole, M. S.; Kleinschek, K. S.; Bele, M.; Jamnik, J.; Gaberscek, M. Flame retardant activity of SiO_2-coated regenerated cellulose fibres. *Polym. Degrad. Stab.* **2007**, *92*, 1957−1965.

(41) Wang, Z.; Wang, Y.; Luo, G. A selective voltammetric method for uric acid detection at b-cyclodextrin modified electrode incorporating carbon nanotubes. *Analyst* **2002**, *127*, 1353−1358.
(42) Huq, R.; Mercier, L. Incorporation of cyclodextrin into mesostructured silica. *Chem. Mater.* **2001**, *13*, 4512−4519.
(43) Grigoriu, A.; Racu, C.; Diaconescu, R. M.; Grigoriu, A.-M. Modeling of the simultaneous process of wet spinning-grafting of bast fibers using artificial neural networks. *Text. Res. J.* **2012**, *82*, 324−335.
(44) Hebeish, A.; Aly, A. A.; El-Shafei, A. M.; Zaghloul, S. Innovative starch derivatives as textile auxiliaries for application in sizing, finishing and flocculation. *Starch/Stärke* **2008**, *60*, 97−109.
(45) Kim, J.; Van der Bruggen, B. The use of nanoparticles in polymeric and ceramic membrane structures: review of manufacturing procedures and performance improvement for water treatment. *Environ. Pollut.* **2010**, *158*, 2335−2349.